Antisymmetric Polar Modes of Thermal Convection in Rotating Spherical Fluid Shells at High Taylor Numbers

Ferran Garcia, Juan Sánchez,* and Marta Net+

Departament de Física Aplicada, Universitat Politècnica de Catalunya, Jordi Girona Salgado 1-3, Campus Nord, Mòdul B4, 08034 Barcelona, Spain

(Received 27 June 2008; published 3 November 2008)

The onset of thermal convection in a rotating spherical shell of intermediate radius ratio $\eta = 0.4$ is studied numerically for Taylor numbers $\mathrm{Ta} \geq 10^{11}$ and the Prandtl number of the liquid sodium ($\sigma = 0.01$). For the first time, it is shown that at very high Taylor numbers the first unstable mode can be antisymmetric with respect to the equator and confined inside a cylinder tangent to the inner sphere at the equator (polar mode). The exponent of the power law determined from the asymptotic dependence of the critical Rayleigh number for very high Ta is 0.57, lower than 2/3, given theoretically for the spiraling columnar modes, and than 0.63, found numerically for the outer equatorially attached modes.

DOI: 10.1103/PhysRevLett.101.194501 PACS numbers: 47.15.−x, 44.25.+f, 47.20.Bp

The thermal convection in fluid spherical shells is a fundamental problem in geophysics and astrophysics. For instance, Earth's magnetic field is generated in its interior by convection driven by thermal and compositional buoyancy. In this way, many of the dynamo features are predetermined by the properties of convection. The large-scale zonal winds observed in the surface of Jupiter at mid- and low latitudes and of Saturn seem to be maintained by deep convection [1]. In the last 20 years, a great quantity of experimental, theoretical, and numerical studies, devoted to improve the understanding of the basic mechanisms which govern the convection in spherical geometry, have appeared. The introductory sections of [2–6], among others, provide good reviews of the state of the art on this subject.

The theoretical paper [7] established that the critical mode for the onset of thermal convection in self-gravitating, and internally heated fluid spheres was a columnar traveling wave, localized around a critical radius $r_i < r_c < r_o$, and symmetric by reflections with respect to the equator. In the inequality r_i and r_o mean the inner and outer radii of the shell. This critical mode fulfills $(v_r, v_\theta, v_\varphi)(r, \theta, \varphi) = (v_r, -v_\theta, v_\varphi)(r, \pi - \theta, \varphi)$ and $\Theta(r, \theta, \varphi) = \Theta(r, \pi - \theta, \varphi)$, where $(v_r,\ v_\theta,\ v_\varphi)$ is the velocity field in spherical coordinates (θ measuring the colatitude), and Θ the temperature perturbation of the conduction state. The validity of this symmetry has been confirmed numerically by several authors, by comparing with the modes obtained for fluid spherical shells of small $\eta = r_i/r_o$, and also in laboratory experiments [8]. Since then, symmetric columnar solutions have been assumed in most of the studies devoted to find or to improve the asymptotic dependence of the onset of instability in spherical shells, independently of its η and of the Prandtl number σ of the fluid. However, there are some ranges of parameters where the latest asymptotic theories in fluid spheres [9] and spherical shells [3] do not apply. For instance, the latter does not fit properly for a small range of η around 0.48 and $\sigma = 1$. As far as we know the reason remains unknown. Moreover, they do not cover small-σ fluids because in fluid spheres and small-η spherical shells the convection sets in with a symmetric pattern, but outer equatorially attached and multicelullar [2,6,10]. So, in a problem with four parameters it is feasible that other kind of modes become preferred, mainly at very high Taylor number, Ta.

The numerical linear stability analysis of the conduction state presented in this Letter shows, for the first time, the existence of antisymmetric modes of convection pre ferred at high Ta in fluid shells of small σ and moderate η, independently of the boundary conditions applied. For these solutions, the velocity field and Θ fulfill $(v_r, v_\theta, v_\varphi)(r, \theta, \varphi) = (-v_r, v_\theta, -v_\varphi)(r, \pi - \theta, \varphi)$ and $\Theta(r, \theta, \varphi) = -\Theta(r, \pi - \theta, \varphi)$. Antisymmetric equatorially trapped inertial waves (solutions of the Poincaré equation) were calculated before by [11], and recently [6] have found numerically preferred antisymmetric thermal Rossby modes filling the shell at moderate Ta.

The Boussinesq approximation of the mass conservation, linear momentum, and energy equations in the rotating frame of reference,

$$\nabla \cdot \mathbf{v} = 0,$$

$$(\partial_t + \mathbf{v} \cdot \nabla)\mathbf{v} = -\nabla \pi + \nabla^2 \mathbf{v} - \mathrm{Ta}^{1/2}\mathbf{k} \times \mathbf{v} + \Theta \mathbf{r},$$

$$\sigma(\partial_t + \mathbf{v} \cdot \nabla)\Theta = \nabla^2 \Theta + (R + \eta(1 - \eta)^{-2} r^{-3} R')\mathbf{r} \cdot \mathbf{v},$$

are solved for a fluid spherical shell rotating about an axis of symmetry with constant angular velocity $\boldsymbol{\Omega} = \Omega \mathbf{k}$, subject to internal or differential heating and radial gravity $\mathbf{g} = -\gamma \mathbf{r}$, where γ is a constant, and $\mathbf{r}$ the position vector. Stress-free $[v_r = \partial_r(v_\theta/r) = \partial_r(v_\varphi/r) = 0]$ or nonslip $(v_r = v_\theta = v_\varphi = 0)$, and perfectly conducting $(\Theta = 0)$ boundaries are employed. Notice that in the formulation the centrifugal force is neglected since in the Earth's outer core and in the major planets $\Omega^2/\gamma \ll 1$, and that the same

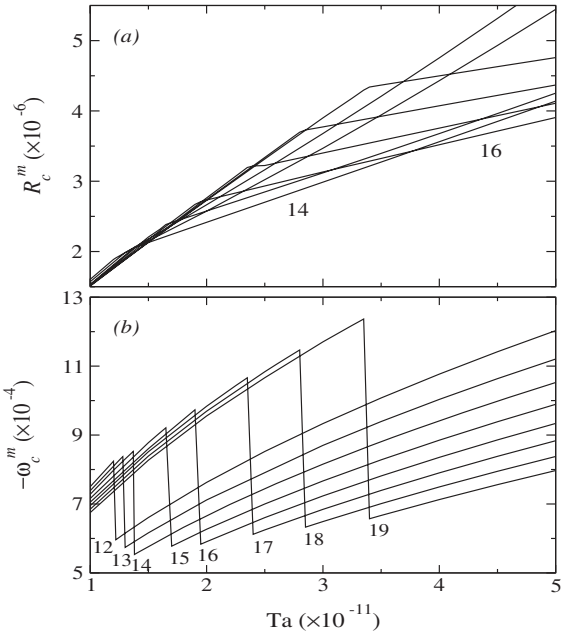

FIG. 1. (a) The critical Rayleigh number R_c^m, and (b) the critical precession frequency $-\omega_c^m$, of each critical mode of azimuthal wave number $m = 12, \ldots, 19$, plotted versus Ta, for $\eta = 0.4$, $\sigma = 0.01$.

units as in [12] are used. The nondimensional Taylor, internal (R) and external (R') Rayleigh and Prandtl numbers are

$$\mathrm{Ta}^{1/2} = \frac{\Omega d^2}{\nu}, \quad R = \frac{q\gamma\alpha d^6}{3c_p\kappa^2\nu}, \quad R' = \frac{\gamma\alpha\Delta T d^4}{\kappa\nu}, \quad \sigma = \frac{\nu}{\kappa},$$

and the conduction state is given by $\mathbf{v} = 0$, and $T_c(r) = T_0 - (R/2\sigma)r^2 + (R'\eta/\sigma(1-\eta)^2)/r$. In the above definitions α means the thermal expansion coefficient, ν the kinematic viscosity, κ the thermal diffusivity, c_p the specific heat at constant pressure, q the rate of heat due to internal sources per unit mass, ΔT the difference of temperature between the inner and outer boundaries due only to differential heating, and $d = r_o - r_i$ the gap width.

The solutions up to $\mathrm{Ta} = 10^{12}$ are computed with the method described in [6], by using 60 radial points, and spherical harmonics of maximal degree 100, but we have checked that, at $\mathrm{Ta} = 5 \times 10^{11}$, an increase of the resolution to 80 by 160 leads to maximal differences of 1.2% in the critical Rayleigh number of the preferred modes of azimuthal wave number m, R_c^m, and of 0.02% in the critical precession frequency ω_c^m. From now on $R' = 0$, unless it is said explicitly.

Figure 1, computed with stress-free boundary conditions, shows the dependence of R_c^m, and ω_c^m on $\mathrm{Ta} > 10^{11}$, for $m = 12, \ldots, 19$. Negative precession frequencies mean that the waves travel in the prograde direction with phase speed $c_m = -\omega_c^m/m$. The changes of slope in Fig. 1(a) and jumps of Fig. 1(b) correspond to the crossing of symmetric outer equatorially attached modes [13] and the antisymmetric modes of Fig. 2 (see figure caption for the meaning of each plot), which spread from the inner to the outer boundaries, but confined inside a cylinder tangent to the inner sphere at the equator (polar modes). The kinetic energy density is almost z independent, as it happens with the spiraling columnar and the equatorially attached modes, although, for the polar solutions, v_φ also depends strongly on z, but its maximum value is less than half that of the other components of the velocity field. The contour plots of Θ are not shown because they resemble very much those of v_r. The main difference is that they are a few degrees out of phase in the φ coordinate.

The envelope of the curves of R_c^m versus Ta gives the critical Rayleigh number R_c, and the preferred pattern of convection. In the range of Ta of Fig. 1, the dominant modes are $m = 17, 18, 14, 16$, successively. At $(\mathrm{Ta}, R_c) = (1.49 \times 10^{11}, 2.13 \times 10^6)$ the $m = 18$ symmetric equatorial mode is superseded by the $m = 14$ antisymmetric polar mode with a decrease of a 31% in $-\omega_c$. We have checked that with nonslip boundaries there is a jump from spiraling columnar to antisymmetric polar modes in the same range of Ta. The eigenfunctions look like that of Fig. 2, with very thin Ekman layers for v_θ and v_φ that stabilize the fluid, rising R_c by 140% at $\mathrm{Ta} = 5 \times 10^{11}$, although the critical precession frequency ω_c decreases hardly by 1.4%. Figure 2 is calculated for stress-free boundary conditions. White means the largest positive velocity and kinetic energy, and the background grey means $\mathbf{v} = 0$ in any case.

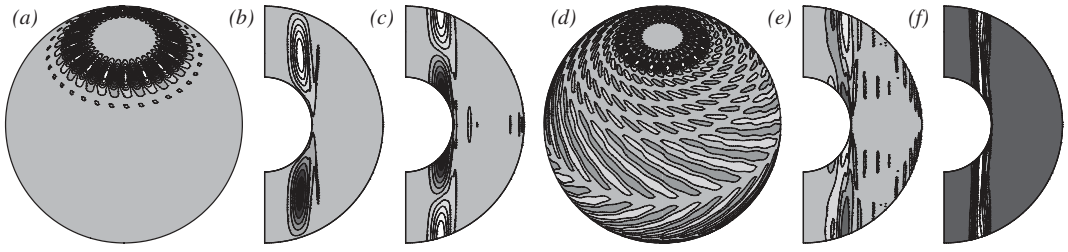

FIG. 2. Preferred antisymmetric polar mode of convection with azimuthal wave number $m = 16$ at $\mathrm{Ta} = 4 \times 10^{11}$, for $\eta = 0.4$, $\sigma = 0.01$. (a), (d) Contour plots of the radial and azimuthal velocities on spheres of radii $r = r_i + 0.50d$ and $r \simeq r_i + 0.99d$, respectively. (b), (c), (e), (f) Contour plots of the radial, colatitudinal, and azimuthal velocities, and of the kinetic energy density on meridional sections, respectively.

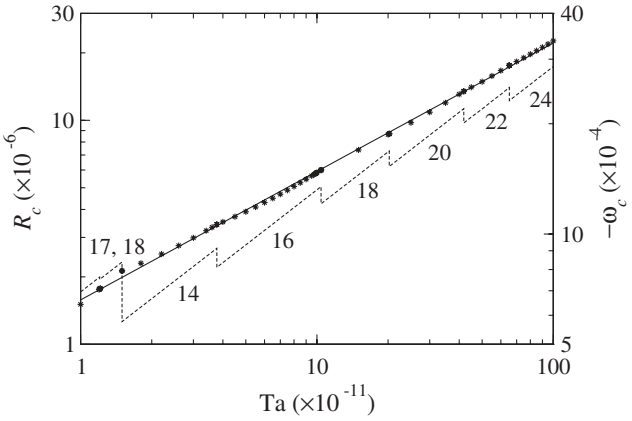

FIG. 3. The critical Rayleigh number R_c, and the critical precession frequency $-\omega_c$ plotted versus Ta, for $\eta = 0.4$, $\sigma = 0.01$. The stars correspond to the computed R_c values, the solid line to its potential fitting, and the dashed line to $-\omega_c$. The left OY axis scales R_c and the right OY axis $-\omega_c$.

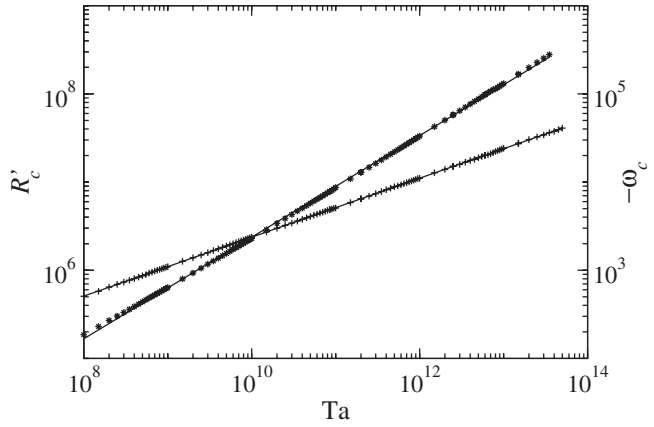

FIG. 4. The critical Rayleigh number R_c', and the critical precession frequency $-\omega_c$ plotted versus Ta, for $\eta = 0.35$, $\sigma = 0.1$, nonslip boundary conditions and differential heating. The stars and plus symbols correspond to the computed R_c' and $-\omega_c$ values, respectively, and the solid lines to their potential fitting. The left OY axis scales R_c' and the right OY axis $-\omega_c$.

To calculate the asymptotic dependence of the critical values, we have increased the degree of the harmonics gradually up to 150 with Ta to maintain the errors into the range determined previously. Figure 3 shows the results. The solid line corresponds to the potential fitting $R_c = 0.78 \times \mathrm{Ta}^{0.57}$, and, although it is not included in the figure because of the jumps among modes, that for $-\omega_c$ gives $\omega_c = -14.21 \times \mathrm{Ta}^{0.33}$. The power 0.57 is clearly lower than $\frac{2}{3}$, the leading order of the asymptotic expansions given theoretically by [3,7,14] for the spiraling columnar modes, and than 0.63, found numerically in [6] for the outer equatorially attached modes. However, it is important to notice that this characteristic is not exclusive of the antisymmetric convection. The same power rules for the inner modes attached to the external part of the tangent cylinder. See, for instance, Fig. 4 computed with the parameters of the outer Earth's core, i.e., with nonslip boundary conditions and differential heating ($R = 0$) for $\eta = 0.35$ and $\sigma = 0.1$. In both cases the flow is restricted to a small portion of the fluid at high latitudes. In contrast to what happens with the equatorially attached modes of the same number of radial cells [6], or with the spiraling columnar modes, in Fig. 3 by increasing Ta, $-\omega_c$ decreases when m increases. In addition, only even modes become preferred. Probably, this fact is due simply to the geometry, since in the case of Fig. 4 the preferred modes are odd for $\mathrm{Ta} > 10^{13}$. Despite these differences, all of them fulfill the power law $\omega_c \propto \mathrm{Ta}^{1/3}$.

Figure 5 shows the internal Rayleigh number R^m and ω^m versus Ta for the two lowest envelopes of the neutral stability curves of $m = 14$ and $m = 16$, again with $\eta = 0.4$ and $\sigma = 0.01$. The solid lines correspond to $m = 14$, and the dashed to $m = 16$. Notice that the thick lines, which are the lowest envelopes for each mode, give the R_c^m and ω_c^m of Fig. 1. The thin lines refer to the second modes in becoming unstable and contributing to the convection. At $\mathrm{Ta} = 10^{11}$ the second eigenfunction is already antisymmetric for $m = 14$ (thin solid line), but symmetric and bicellular for $m = 16$ (thin dashed line). The curve of bicellular modes cross that of antisymmetric modes at $\mathrm{Ta} = 1.28 \times 10^{11}$. In both cases ($m = 14$, 16), by increasing R^m the new interchange of eigenfunctions takes place in the opposite way than following the thick curves, i.e., the

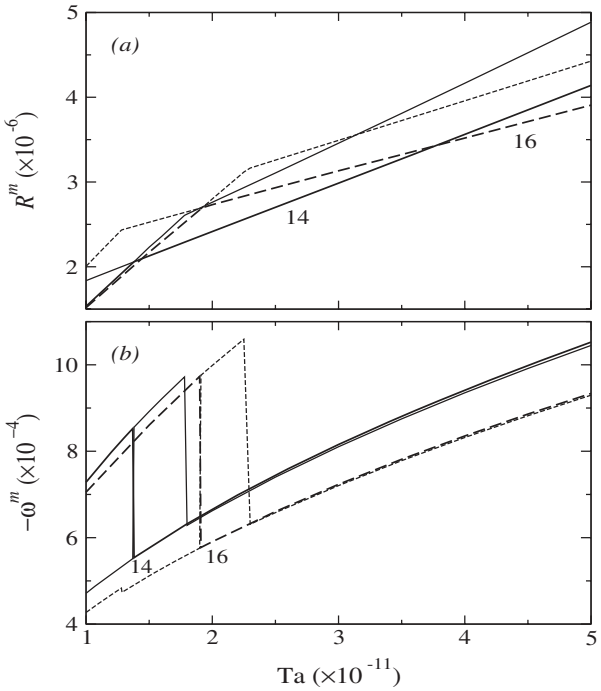

FIG. 5. (a) The Rayleigh number R^m, and (b) the precession frequency $-\omega^m$, of the first and second envelopes of the neutral stability curves of $m = 14$, and $m = 16$, plotted versus Ta, for $\eta = 0.4$, $\sigma = 0.01$.

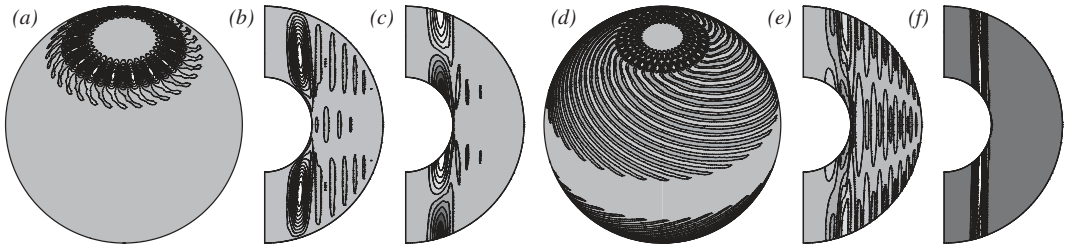

FIG. 6. Symmetric polar mode of convection with azimuthal wave number $m = 16$ at $\mathrm{Ta} = 4 \times 10^{11}$, for $\eta = 0.4$, $\sigma = 0.01$. Same contour plots as in Fig. 2.

antisymmetric polar modes are superseded by those equatorially trapped [15]. However, the latter are soon replaced by polar symmetric modes (see Fig. 6), at $\mathrm{Ta} \simeq 1.78 \times 10^{11}$ for $m = 14$, and at $\mathrm{Ta} \simeq 2.27 \times 10^{11}$ for $m = 16$. We have checked that it is so at least up to $\mathrm{Ta} = 10^{13}$. The two types of polar solutions have the kinetic energy density confined between $\theta \simeq 13°$ and $\theta \simeq 21°$, remaining almost z independent. In addition their phase speeds differ less than 0.5%, but the Rayleigh number of the symmetric solutions increases by 12%.

In this Letter we have reported the existence of preferred polar antisymmetric modes of thermal convection, and determined numerically the power law dependence of R_c with Ta. Moreover, from the preceding results we can conclude that, although we have not found preferred symmetric polar modes, it is possible they become critical for other parameters. Furthermore, the same could happen with other families of modes, not shown in this Letter, but found at not very high R. For instance, the third and fourth preferred eigenfunctions for $m = 18$ at $\mathrm{Ta} = 2 \times 10^{12}$ are antisymmetric and symmetric polar bicellular modes, respectively. We have also detected antisymmetric equatorially trapped modes similar to the inertial waves of [11], and tri- and quadricellular modes like those described in [16].

Assuming the equatorial symmetry in the study of low-σ convection in spherical geometries of moderate η can lead to wrong solutions, although they can be indistinguishable from the real flows when they are observed from a pole (compare Figs. 2 and 6).

The nonpreferred modes of convection may also contribute to nonlinear flows. The superposition of the polar symmetric and antisymmetric nonlinear waves may give rise to coherent polygonal structures without equatorial symmetry, of the type observed in the north pole of Saturn.

Finally, the preceding results motivate the study of the *laminar* nonlinear dynamics of the polar flows, and their implication in the generation of planetary and stellar magnetic fields. The polar convection is known to grow in strongly nonlinear regimes [17,18]. However, our preliminary nonlinear results indicate the existence of polar antisymmetric flows at very low Rayleigh numbers.

This work is supported by Spain MEC-DGI, and Catalonia GENCAT under Grants No. FIS2007-64993 and No. 2005SGR01028, respectively.

*sanchez@fa.upc.edu
+marta@fa.upc.edu

[1] D. H. Atkinson, J. B. Pollack, and A. Seiff, J. Geophys. Res. **103**, 22 911 (1998).
[2] K. Zhang and X. Liao, J. Fluid Mech. **518**, 319 (2004).
[3] E. Dormy, A. M. Soward, C. A. Jones, D. Jault, and P. Cardin, J. Fluid Mech. **501**, 43 (2004).
[4] N. Gillet and C. A. Jones, J. Fluid Mech. **554**, 343 (2006).
[5] N. Gillet, D. Brito, D. Jault, and H.-C. Nataf, J. Fluid Mech. **580**, 83 (2007).
[6] M. Net, F. Garcia, and J. Sánchez, J. Fluid Mech. **601**, 317 (2008).
[7] F. H. Busse, J. Fluid Mech. **44**, 441 (1970).
[8] C. R. Carrigan and F. H. Busse, J. Fluid Mech. **126**, 287 (1983).
[9] C. A. Jones, A. M. Soward, and A. I. Mussa, J. Fluid Mech. **405**, 157 (2000).
[10] K. Zhang, X. Liao, and F. H. Busse, J. Fluid Mech. **578**, 371 (2007).
[11] K. Zhang, J. Fluid Mech. **248**, 203 (1993).
[12] R. Simitev and F. H. Busse, New J. Phys. **5**, 97 (2003).
[13] K. Zhang, J. Fluid Mech. **268**, 211 (1994).
[14] P. H. Roberts, Phil. Trans. R. Soc. A **263**, 93 (1968).
[15] K. Zhang, J. Fluid Mech. **284**, 239 (1995).
[16] M. Ardes, F. H. Busse, and J. Wicht, Phys. Earth Planet. Inter. **99**, 55 (1997).
[17] P. Olson and J. Aurnou, Nature (London) **402**, 170 (1999).
[18] U. R. Christensen, J. Fluid Mech. **470**, 115 (2002).